Magnetic Properties of Reduced and Re-oxidized Mn-Na_2WO_4/SiO_2: A Catalyst for Oxidative Coupling of Methane (OCM)

Wiebke Riedel[1,2], Lukas Thum[3], Jannik Möser[2,4], Vinzenz Fleischer[3], Ulla Simon[5], Konrad Siemensmeyer[6], Alexander Schnegg[2,4], Reinhard Schomäcker[3], Thomas Risse[1,2], Klaus-Peter Dinse[7]*

[1]Institut für Chemie, Freie Universität Berlin, Takustraße 3, 14195 Berlin, Germany.

[2]Joint EPR Lab, Berlin, Germany.

[3]Institut für Chemie, Technische Universität Berlin, Straße des 17. Juni 124, 10623 Berlin, Germany.

[4]Insititut Nanospektroskopie, Helmholtz-Zentrum Berlin, Kekuléstraße 5, 12489 Berlin, Germany.

[5]Fachgebiet Keramische Werkstoffe, Institut für Werkstoffwissenschaften und -technologien, Fakultät III, Technische Universität Berlin, Hardenbergstr. 40, 10623 Berlin, Germany.

[6]Institut Quantenphänomene in neuen Materialien, Helmholtz-Zentrum Berlin, Hahn-Meitner-Platz 1, 14109 Berlin, Germany.

[7]Fachbereich Physik, Freie Universität Berlin, Arnimallee 14, 14195 Berlin, Germany.

ABSTRACT: The magnetic properties of Mn-Na_2WO_4/SiO_2, a promising catalyst for the oxidative coupling of methane (OCM), were investigated in two states: reduced with CH_4 until reactivity ceased and re-oxidized with O_2 to probe for state-specific magnetic species and their involvement in the oxygen storage of the catalyst. Employing temperature and frequency dependent continuous wave (cw) and pulsed Electron Paramagnetic Resonance (EPR) spectroscopy combined with SQUID (Superconducting Quantum Interference Device) magnetization measurements, allowed to identify a variety of Mn species in different oxidation

states and their role in the oxygen storage capability of the catalyst. For the re-oxidized catalyst, formation of magnetically ordered Mn(II) and Mn(III) containing Mn_3O_4 as well as Mn_2O_3 and/or $MnMn_6SiO_{12}$ phases were detected. The reduced catalyst exhibits almost ideal paramagnetic behavior and a strong, broad cw EPR signal consistent with the formation of short-range ordered nano-sized Mn(II) oxide demonstrating the involvement of these Mn species in the oxygen storage capability of the catalyst. In contrast, rather isolated, highly oxidized Mn(IV) as well as different Mn(III) species were observed by pulsed EPR which are not affected by the oxidation state of the Mn-Na_2WO_4/SiO_2 catalyst suggesting an inaccessible, buried location, presumably in the SiO_2 support. Furthermore, paramagnetic sites with an effective S = ½ spin are detected, whose intensity depends on the oxidation state of the sample and are thus involved in the oxygen storage capacity of the catalyst.

1. INTRODUCTION

Mn-Na_2WO_4/SiO_2 was first introduced by Fang et al.[1-2] as a promising catalyst for the oxidative coupling of methane (OCM) to chemically more valuable C_2 compounds, such as ethane (C_2H_6) or ethene (C_2H_4, see eq. 1).

$$2\ CH_4 + O_2 \rightarrow C_2H_4 + 2\ H_2O \quad (1)$$

In previous studies, CH_4 conversions of up to 20-30 % and a C_2 selectivity of 70-80 % were reported for this catalyst as well as a long term stability of several hundred hours under high performance conditions.[3-4] For elucidation of the catalytic mechanism on the molecular level the so called “chemical looping” concept was introduced, which aims at separating the contact of methane and oxygen with the catalyst temporarily.[5] The concept requires the ability of the catalyst to store oxygen while in contact with molecular oxygen, which is subsequently utilized during the admission of methane. Due to the presence of reducible oxides, the Mn-Na_2WO_4/SiO_2

catalyst exhibits oxygen storage capabilities allowing for conversion of methane (CH_4) in the absence of molecular oxygen in the feed.[5] In chemical looping experiments, the catalyst is reversibly cycled between an oxidized and a reduced state, which renders the nature of these states important for an understanding of the catalyst as well as for its rational improvement.[5-6] The analysis of the compositional changes within the complex multi-component Mn-Na_2WO_4/SiO_2 catalyst is challenging and a variety of characterization techniques have been employed.[3, 7-8] Wu et al. suggested a reaction mechanism with W(VI) being reduced to W(IV) and re-oxidized by gas-phase oxygen to W(VI) based on Raman and cw EPR results,[7-8] while later a more complex mechanism involving W(VI) and W(V) as well as Mn(III) and Mn(II) was proposed.[3] However, no direct evidence for the presence of reduced W species could be identified spectroscopically.[3, 7-8] Based on X-Ray Diffraction (XRD) results, Sadjadi et al. confirmed the presence of Mn_2O_3 and Na_2WO_4 phases for the re-oxidized catalyst. In contrast to that, the reduced catalyst exhibits a $MnWO_4$ phase, but no indication for Mn_2O_3 could be found.[4] The satellite structure in the Mn 2p region of the XPS (X-ray Photoelectron Spectroscopy) spectrum suggests the presence of Mn(II)O, however, the corresponding crystalline phases have to be either small or very defective precluding their observation by XRD.[6] As the catalyst contains under reaction conditions a molten phase,[6] the structural properties for samples investigated at low temperatures may differ, but the observed phase changes for the reduced and re-oxidized catalyst are in line with a change in oxidation state of Mn during the chemical looping cycle. A broad cw EPR signal centered around g = 2.01 observed for the reduced catalyst was attributed to a reduction of Mn(III) to Mn(II).[8] Catalytic studies were able to correlate the oxygen storage capacity with the Mn content and found an optimal thickness of the Mn loading, which suggests that not just the outermost layer of Mn-Na_2WO_4 is involved in the reduction by CH_4.[6, 9-10] This observation is in line with expectations based on the presence of a molten phase of

Mn-Na_2WO_4 under reaction conditions. Our present study aims at gaining additional insight into the changes in chemical composition during the redox cycle of a chemical looping experiment. As Mn was found to play a central role in these processes, we probed the magnetic properties of the multi-component Mn-Na_2WO_4/SiO_2 catalyst focusing on two states corresponding to the starting and end point of methane admission during the chemical looping experiment to further elucidate the nature of the species involved in the oxygen storage capability of the catalyst. We investigated a Mn-Na_2WO_4/SiO_2 catalyst with 4 wt.% Na_2WO_4 and 2 wt.% Mn loading (average layer thickness 8.6 nm)[6] on a silica gel support, which has shown high activity in chemical looping experiments.[6] We will compare (a) a reduced state of the catalyst by reaction with CH_4 until reactivity ceased and (b) a re-oxidized one using O_2 as applied during the chemical looping process. For the spectroscopic analysis, temperature and frequency dependent cw as well as pulsed EPR techniques are combined with complementary temperature dependent magnetization measurements thereby probing for different paramagnetic species as well as for characteristic magnetic phase transitions as expected for different Mn-containing oxide phases.

2. EXPERIMENTAL METHODS

The catalysts were synthesized following procedures similar to those described previously in detail elsewhere allowing for production of large catalysts amounts and yielding comparable catalytic activity to catalysts prepared with incipient wetness impregnation method.[11] In this study, the SiO_2 support (Davisil 636, Sigma Aldrich, particle size 150-350 μm) was coated with $Mn(NO_3)_2$ and Na_2WO_4 aqueous precursor solutions yielding catalyst loadings of 4 wt.% Na_2WO_4 and 2 wt.% Mn and a specific surface area of 1.9 m^2/g after calcination at 800 °C for 8 h in air. The as prepared catalysts were initially heated up to 775 °C (10 °C/min) in a flow of 20 % O_2 in He. During the heating, the catalyst was purged at 700 °C, 725 °C and 750 °C with He for

5 min and subsequently exposed to 1 mL of 30 % CH_4 in He. A total flow of 30 mL/min was used for an inner reactor diameter of 8 mm, a height of the catalyst bed of approx. 20 mm and catalyst mass of 0.57 g yielding thus a contact time of 0.05 $L \cdot g^{-1} \cdot min^{-1}$. After the last heating step to 775 °C in 20% O_2 in He, the catalyst was purged with pure He until mass spectrometer signals due to O_2 vanished. This procedure was applied to ensure a defined state of the catalyst at the beginning of the reduction and re-oxidation conducted at 775 °C. The reaction temperature of 775 °C was chosen to be well above the temperature where phase transformation to a molten state occurs (approx. 600 °C), but well below the temperature where decomposition begins (approx. 830 °C).[12-14] For preparation of the reduced samples, the catalyst was subsequently reacted at 775 °C with 30 % CH_4 in He, until all signals due to C_2 products as well as H_2O, CO and CO_2 vanished. For the re-oxidized samples, the catalyst was additionally purged in He for 5 min and subsequently reacted at 775 °C in 20 % O_2 in He for 10 min. The O_2 exposure was chosen based on previous chemical looping experiments to achieve a full re-oxidation of the catalyst.[6] After reaction, the samples were cooled in a flow of pure He and directly sealed off in the quartz tubes used for EPR experiments. Two sets of samples were prepared. For 34 GHz and 9.8 GHz EPR measurements samples were sealed in 2.9 mm outer diameter tubes, while 5 mm outer diameter tubes were used for 263 GHz and some 9.8 GHz EPR investigations as well as for the magnetization measurements. For the samples sealed off under inert gas (He) no significant change in the EPR spectra over time was observed demonstrating their stability under these conditions.

Magnetization measurements were conducted using a SQUID-based magnetometer (MPMS 3, Quantum Design) at the Quantum Materials Core Lab at Helmholtz Zentrum Berlin. The sealed samples from EPR measurements were mounted in a drinking straw. Because the samples were quite long (~20 mm) compared to the size of the SQUID pick up system the measurements were

conducted in DC mode and analysed offline to obtain the magnetization change as a function of temperature and field. While an absolute calibration of the magnetic moment was not attempted for these samples, using the identical samples as in the EPR measurements allowed for a direct qualitative comparison of the EPR and magnetization results. It should be noted that the EPR spectra were re-measured after the magnetization measurements indicating no significant changes compared to the spectra taken before the magnetization measurements. The background for the magnetization measurements has been checked with an empty quartz tube yielding only a slowly varying diamagnetic signal without distinct features. The magnetization was measured at temperatures ranging between 5 K and 300 K applying magnetic fields up to 7 T. Both field cooled (FC) and zero field cooled (ZFC) magnetization curves were measured as a function of temperature.

For pulsed and cw EPR measurements at different mw frequencies, i.e. 9.8, 34 and 263 GHz, various setups were employed. For room temperature cw EPR spectra at X-band frequencies (9.8 GHz) a Bruker B-ER420 spectrometer upgraded with a Bruker ECS 041XG microwave bridge and a lock-in amplifier (Bruker ER023M) was employed using a Bruker SHQ or a Bruker TE_{102} resonator for samples sealed in quartz tubes of 2.9 mm or 5 mm outer diameter, respectively. Echo-detected and cw 9.8 GHz EPR measurements at low temperatures were conducted with a Bruker ElexySys 680 setup equipped with an Oxford helium cryostat using a commercial Bruker Flexline ENDOR probe head. The field-swept echo (FSE) spectra at 9.8 GHz were recorded using a two pulse “Hahn-echo” mw sequence (20-300-40 ns) at a temperature of 20 K yielding an absorptive type of spectrum. For cw Q-band (34 GHz) EPR measurements at room temperature, a Bruker B-ER420 spectrometer upgraded with a Bruker ER051 QG microwave bridge and a lock-in amplifier (Bruker ER023M) using a ER051QT resonator was employed. Echo-detected pulsed EPR measurements at Q-band frequencies were conducted on a Bruker ElexSys 580 setup with a

home-built cavity (F. Lendtzian, TU Berlin). FSE spectra at 34 GHz were recorded using a two pulse mw sequence (16-250-32 ns). Transient nutation (TN) measurements at 34 GHz were conducted applying a PEANUT (Phase-inverted Echo-Amplitude detected Nutation) pulse mw sequence[15] with a $\pi/2$ pulse length of 32 ns, a delay time τ of 200 ns and a high turning angle (HTA_x) pulse of 2048 ns. Phase inversion time within the high turning angle (HTA_x) pulse was incremented by 2 ns starting with an initial inversion after 32 ns.[15] For 34 GHz HYSCORE (Hyperfine Sub-level Correlation) measurements, a $\pi/2$ pulse length of 16 ns, and a delay time τ of 150 ns between the first pulses was used.[16] The ENDOR (Electron Nuclear Double Resonance) spectra were recorded applying a Mims pulse sequence with a $\pi/2$ pulse length of 20 ns, delay time τ of 200 ns and a rf π pulse length of 80 μs. 263 GHz cw EPR measurements were performed in a Bruker ElyxSys 780 (263 GHz, 12 T) spectrometer equipped with a non-resonant sample insert, and a He cooled cryostat.

Further compositional, structural as well as catalytic analysis of this catalyst has been previously described in detail.[6]

3. RESULTS AND DISCUSSION

The 34 GHz cw EPR spectra of the reduced and the re-oxidized silica gel supported Mn-Na_2WO_4 catalyst obtained at room temperature are displayed in Figure 1. The catalyst reduced with CH_4 exhibits a strong, broad signal at g = 2.0 with a line width of about 50 mT. In contrast, the re-oxidized catalyst exhibits a cw EPR signal of much smaller amplitude. This is in good agreement with previous EPR results attributing the strong cw EPR signal in the reduced catalyst to formation of Mn(II) species.[8] The cw EPR signals of the reduced and re-oxidized Mn-Na_2WO_4/SiO_2 catalyst differ not only in signal amplitude, but also in line shape: Whereas the peak observed for the reduced sample can be approximated with a single Lorentzian line, at least

two Lorentzian lines are required to fit the signal of the re-oxidized sample reasonably well as displayed in Figure 1b. One of the lines is similar to the one observed for the reduced sample, while the second one is considerably broader indicating that the paramagnetic species detected by cw EPR are strongly affected by the redox reaction. While the peak amplitudes of the EPR signals differ by roughly an oder of magnitude, it is important to note that the EPR susceptibility of the reoxidized sample is quite comparable due to the broad signal, which contributes more than 90 % to the signal. To gain further information on these paramagnetic species formed by reduction cw EPR measurements at different mw frequencies were performed. Figure 2 shows the 9.8 GHz and 263 GHz cw EPR spectra of the reduced catalyst at room temperature. Despite the large change in mw frequency, the measured peak to peak line width (ΔB_{pp}) remains almost constant excluding significant contribution of anisotropic Zeeman interaction to the line width. Probably spin-spin coupling is the dominant broadening mechanism, as expected for highly concentrated spin systems such as found in Mn(II) oxide or $MnWO_4$ nanoparticles. [17-20]

For further indentification of the cw EPR signals seen for reduced and re-oxidized samples the temperature dependence of line widths and double integrated intensities was studied. As discussed in detail in the Supporting Information, for the re-oxidized sample a significant deviation from the Curie behavior expected for isolated paramagnetic centers is observed in the range of 100 K and 80 K. Combined with a change in line shape, this implies that in the re-oxidized catalyst the EPR signal of at least one of the centers decreases in this temperature range. A possible reason for the loss in EPR signal is an anti-ferromagnetic phase transition with a Néel temperature in this range.

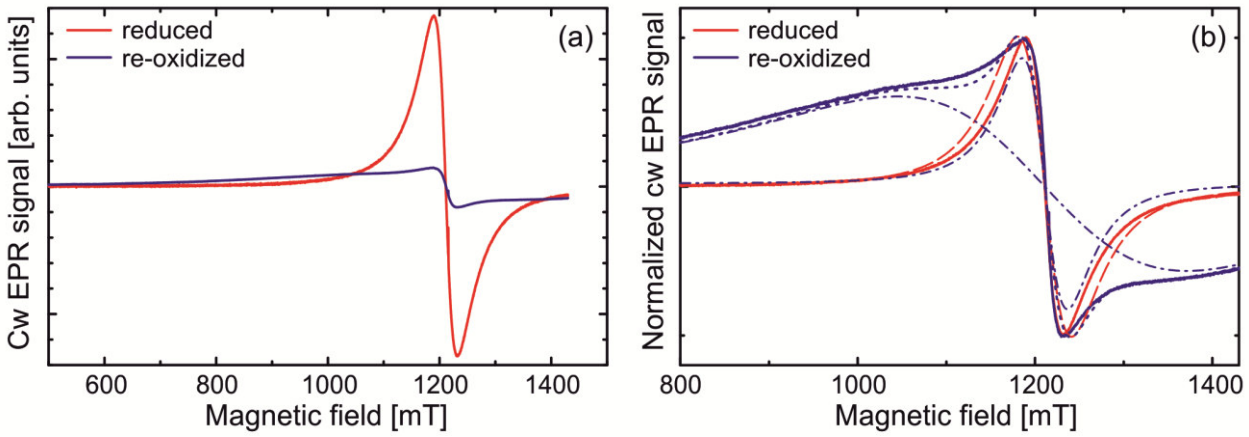

Figure 1. 34 GHz cw EPR spectra recorded at room temperature for the reduced (red) and re-oxidized (blue) Mn-Na_2WO_4/SiO_2 catalyst (1 mT modulation amplitude, 100 kHz modulation frequency); (b) comparison of the peak normalized experimental spectra (solid lines) shown in (a) to fits using one or two Lorentzian lines for the reduced (dashed line) and the re-oxidized (dotted line: sum of two Lorentzian lines; dash-dot lines: individual Lorentzian lines) sample, respectively.

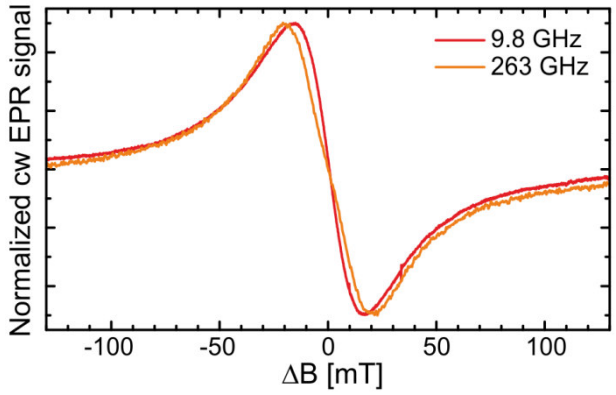

Figure 2. Comparison of 9.8 GHz and 263 GHz cw EPR spectra of the reduced Mn-Na_2WO_4/SiO_2 catalyst measured at room temperature (Magnetic field axis were shifted such that the field values of the zero crossing were set to zero).

For further confirmation, temperature dependent magnetization measurements were performed aiming at an identification of phase transitions expected for various manganese oxide phases.

Results are depicted in Figure 3. The re-oxidized Mn-Na_2WO_4/SiO_2 catalyst exhibits a broad anti-ferromagnetic phase transition around T_N = 90 K as well as a second, much weaker ferromagnetic phase transition around T_C = 45 K, which becomes less pronounced as the magnetic field is increased (data not shown). It should be noted that also a paramagnetic component appears to persist at low temperatures in the re-oxidized sample. These results agree with the measured temperature dependence of the cw EPR spectra (see Figure S2). The ferromagnetic phase transition at 45 K is in good agreement with the Curie temperature of ferrimagnetic (bulk) Mn_3O_4 (T_C = 42 K),[21-22] but is also in rough agreement with the Curie temperature reported for alkali-doped α-MnO_2 ranging between 44 K and 60 K, depending on the doping concentration.[23] In a previous XRD study of the re-oxidized Mn-Na_2WO_4/SiO_2 catalyst, neither the presence of a Mn_3O_4 phase nor the formation of an α-MnO_2 phase could be clearly shown.[4] However, MnO_2 is expected to be largely converted to Mn_3O_4 under reaction conditions with an applied O_2 pressure of approx. 200 mbar and reaction temperature of 775 °C.[24-25] Therefore, the signal at T_C = 45 K is assigned to Mn(II) and Mn(III) containing Mn_3O_4. The antiferromagnetic phase transition at T_N = 90 K is consistent with Mn_2O_3 exhibiting a bulk Néel temperature of 80 K as well as with $MnMn_6SiO_{12}$ with a bulk Néel temperature of 93 K.[26-30] For β-MnO_2 with a bulk Néel temperature of 92 K,[31-32] as previously noted, a conversion to Mn_2O_3 and/or Mn_3O_4 is expected under re-oxidation conditions with the applied oxygen pressure and reaction temperature of 775 °C.[24-25] Moreover, a previous XRD and NEXAFS study suggested the presence of Mn_2O_3 and/or $MnMn_6SiO_{12}$ in the re-oxidized Mn-Na_2WO_4/SiO_2 catalyst, while no clear indication for MnO_2 was observed in the samples.[4] Therefore, the signal at T_N = 90 K is assigned to nano-sized Mn(III) containing Mn_2O_3 and/or Mn(II) and Mn(III) containing $MnMn_6SiO_{12}$ exhibiting a slightly different Néel temperature as compared to the bulk material due to the size of the phases.

In contrast, the reduced Mn-Na_2WO_4/SiO_2 catalyst exhibits an almost ideal Curie behavior as expected for a paramagnetic sample. Except for a very weak signal around 25 K, which might be indicative for a magnetic phase transition at this temperature, the curve lacks characteristic features pointing to a magnetically ordered phase. A transition temperature of 25 K would be consistent with a spin glasses like behavior observed in manganese oxides.[23, 33-34] Ferrimagnetic Mn_3O_4 is a (partially) reduced manganese oxide that is in line with expectations for the reduced catalyst known to contain Mn_2O_3 and/or $MnMn_6SiO_{12}$ in the re-oxidized state. However, the magnetization curve lacks indication for a ferri-magnetic Mn_3O_4 phase, which should show a Curie temperature around T_C = 42 K.[21-22] Based on the satellite structure of the Mn 2p XPS signal Mn was previously assigned to Mn(II)O which does not exclude the presence of (magnetically disordered) Mn_3O_4.[6, 35] Antiferromagnetically ordered, crystalline MnO exhibits a Néel temperature of T_N = 117 K (bulk)[36] which may vary depending on particle size and the presence of other (magnetic) phases.[17-19] Yet, no evidence for such a magnetic transition was found rendering the presence of crystalline MnO unlikely, which is in line with the XRD results.[4] Amorphous MnO encapsulated in a glass matrix was found to lack a paramagnetic to antiferromagnetic phase transition. The magnetization of these particles show, however, a significant deviation from a simple Curie behavior, which complicates a simple assignment, yet, no indication for such deviations could be found for the present sample.[18]

Previous XRD studies identified a $MnWO_4$ phase in the reduced Mn-Na_2WO_4/SiO_2 catalyst, however, the diffraction spots were broad indicating either small or highly defective crystallites.[4] EPR studies of $MnWO_4$ are scarce, but the room temperature signal observed here is compatible with the presence of $MnWO_4$.[20] Single crystalline $MnWO_4$ exhibits a paramagnetic to anti-ferromagnetic phase transition in the range of 10-15 K, which is not seen in the magnetization measurements.[37-41] Even though a clear indication for magnetic phase transition is missing, the

behavior of the cw EPR line width (see Figure S1) is in line with an increase of the spin-spin interaction, which typically leads to a divergence of the line width at the Néel temperature for antiferromagnetically ordered systems, as observed for Mn(II) oxide nanoclusters.[17-19] Given the sensitivity of magnetic order on structural imperfections and the broad reflexes found in XRD, the lack of corresponding phase transitions does not exclude the presence of a $MnWO_4$ phase. In combination with the XPS and XRD results reported in literature, the broad cw EPR signal observed for the reduced sample can be tentatively assigned to a mixture of amorphous MnO and defected $MnWO_4$ phases.

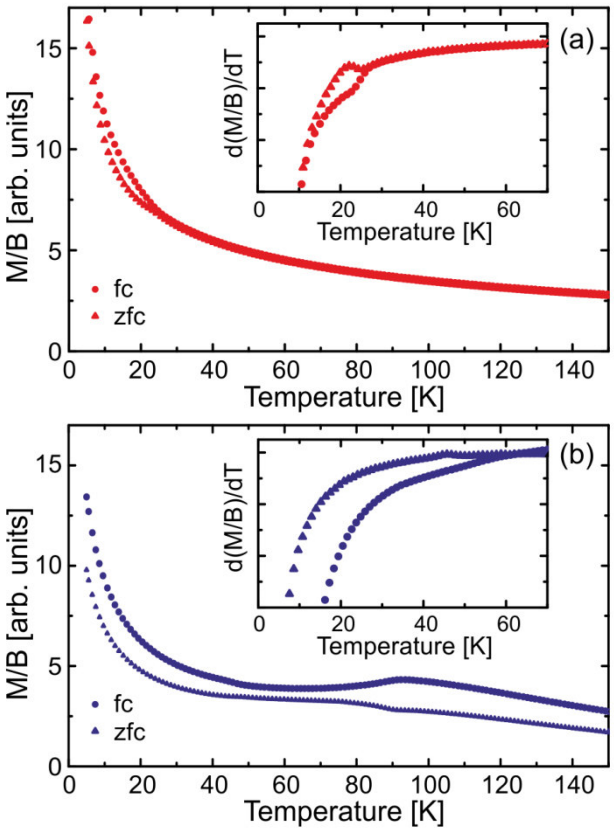

Figure 3. FC and ZFC temperature dependent magnetization measurements of the (a) reduced and (b) re-oxidized Mn-Na_2WO_4/SiO_2 catalyst. Insets show the derivate curves d(M/B)/dT. The measurements were conducted at a magnetic field of 10 mT.

Similar to the cw EPR measurements, the magnetization measurements reveal a clear difference between the two states of the catalyst: While the reduced Mn-Na_2WO_4/SiO_2 catalyst exhibits almost ideal Curie behavior indicative for paramagnetic species, re-oxidation of the catalyst results in the formation of magnetically ordered phases contributing considerably to the overall magnetic susceptibility. Already thin films/small particles (5-10 nm) of manganese oxides being comparable to the dimensions of the Mn-Na_2WO_4 layer (average thickness of 8.6 nm[6]) on the silica support used here, were shown to exhibit magnetic ordering.[17, 19, 34, 42-45] Apparently, the formation of long-range ordered magnetic phases reports on a massive restructuring of the catalyst depending on its oxidation state affecting a large part of the Mn-Na_2WO_4 layer.

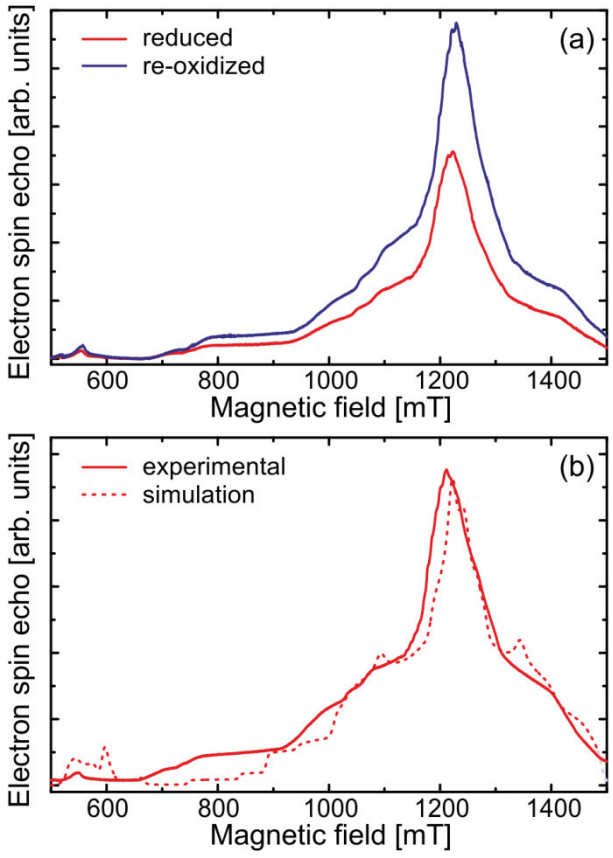

Figure 4. (a) 34 GHz FSE spectra at 20 K of the reduced and re-oxidized Mn-Na_2WO_4/SiO_2 catalyst, (b) comparison of experimental spectrum of reduced catalyst with simulations for an S = 2 species.

The strong cw EPR signal in the reduced sample previously assigned to Mn(II)[8] in combination with the formation of long-range magnetically ordered Mn(III) containing oxides upon re-oxidation provide clear experimental evidence for the oxygen storage capacity of manganes oxides in the catalyst. Upon cooling the reduced Mn-Na_2WO_4/SiO_2 catalyst from the reaction temperature of 775 °C to room temperature, disordered or defect-rich Mn(II) containing phases such as MnO or $MnWO_4$ are formed, which do not form long-range magnetically ordered phases. However, they exhibit sufficiently short distances between the magnetic Mn centers resulting in significant spin-spin interaction, which explains the observed cw EPR results.

The cw EPR spectra were found to be dominated by signals indicative for strong spin-spin coupling within the system. Previous experimental results have suggested that apart from the oxygen storage capacity of the Mn containing phase the system undergoes additional transformations such as the Na induced recrystallization of the silica support into an α-cristobalite phase.[1-2, 11, 46] In addition, the participation of W(V) species was discussed,[3, 7-8] which poses the question if additional paramagnetic species can be identified in these systems, which can shed some light on these processes. To this end, pulsed EPR experiments were performed, which act as a filter removing all species with short T_2 relaxation times compared to the pulse separation (200 ns). Figure 4a displays the 34 GHz field swept echo (FSE) spectra of the reduced and re-oxidized catalyst. In sharp contrast to the cw EPR spectra (Figure 1), both samples exhibit a broad signal with very similar shape and a maximum intensity at 1220 mT ($g \approx 2$). The intensity of the FSE signal is increased after re-oxidation with O_2. Because T_1 and T_2 relaxation times were found to be similar for both samples, the signal increase can be associated with a higher concentration of these species in the re-oxidized catalyst. This shows that cw and pulse EPR spectroscopy detect different species. Hence, the absence of the strong cw EPR signal dominating the low temperature spectrum of the reduced catalyst in the FSE spectra corroborates a strong

spin-spin interaction between the Mn(II) centers, as expected for Mn(II) containing oxides (MnO or $MnWO_4$) alike, which typically result in short T_2 relaxation times.

The broad FSE detected signal can be simulated using EasySpin[47] assuming an ensemble of isolated S = 2 systems, as expected for individual high-spin Mn(III) species. The best fit was achieved with g = 1.97, B_{20} = 430 MHz, B_{22} = 800 MHz, B_{40} = 20 MHz and B_{44} = 720 MHz as depicted in Figure 4b. It should be noted that the FSE spectra of the samples taken at 9.7 GHz (not shown) could be fitted with very similar parameters supporting the assignment of the signal to an S = 2 species.

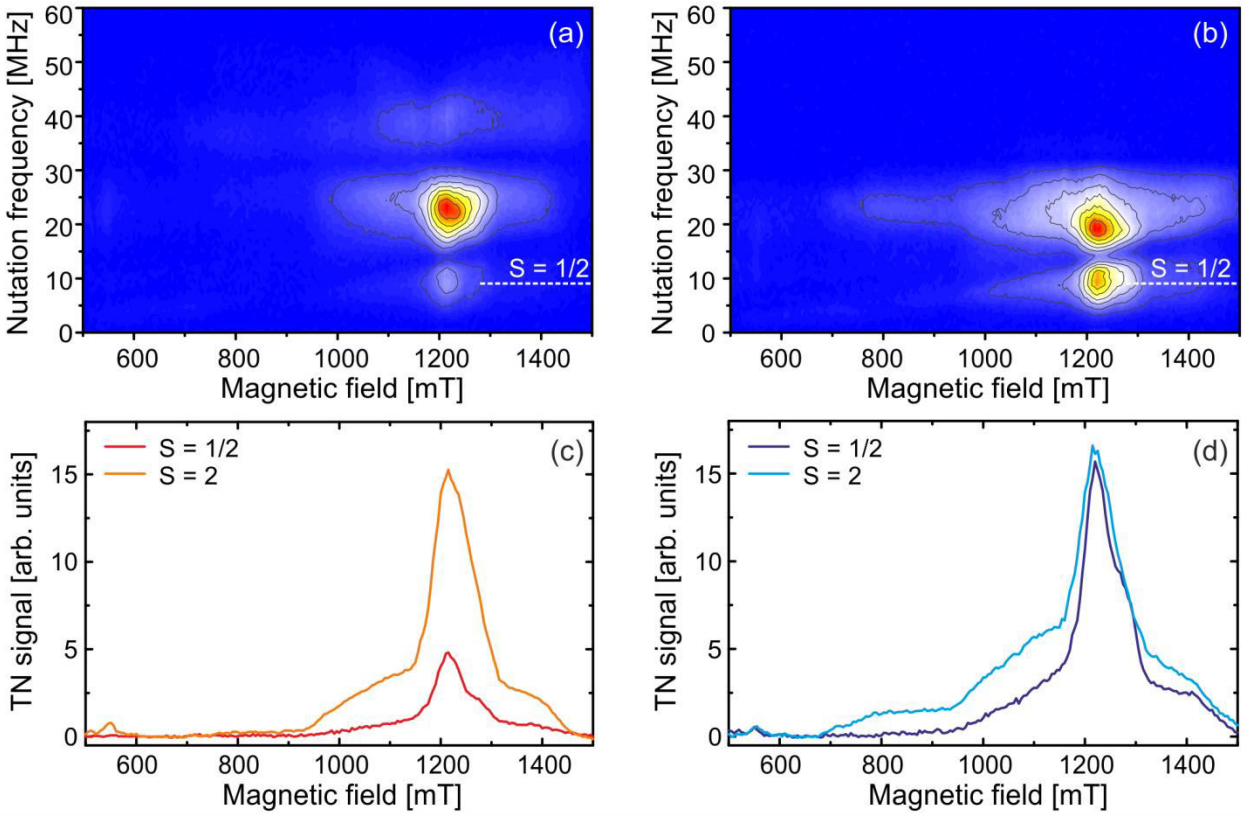

Figure 5. 34 GHz transient nutation measurements at 20 K of (a) the reduced and (b) the re-oxidized Mn-Na_2WO_4/SiO_2 catalyst. Spectra in the nutation frequency range of the S = ½ and S = 2 species for (c) the reduced and (d) the re-oxidized catalyst.

To further confirm the S = 2 nature of the spin center, 34 GHz 2D transient nutation (TN) measurements were conducted using the PEANUT sequence.[15] Transient nutation spectroscopy allows to identify the effective spin of paramagnetic species, which in turn can be used to identify the oxidation state of the metal center. This method can be applied for disordered systems, as shown recently.[48-49] Figure 5 shows the transient nutation spectra of the reduced and the re-oxidized catalyst obtained under identical measurement conditions. Both the reduced and the re-oxidized samples exhibit similar TN spectra with two main features along the transient nutation axis: One maximum at a nutation frequency of around 20 MHz and a second signal with a nutation frequency of 9.5 MHz. The peak at $g \approx 2$ with $\nu_{TN} = 9.5$ MHz is assigned to a S = ½ species of as yet unknown origin. This assignment was verified in a separate measurement of a coal reference (S = ½) together with the re-oxidized catalyst, demonstrating an identical nutation frequency for the coal reference and the S = ½ species observed in the spectra of the Mn-Na_2WO_4/SiO_2 catalyst (data not shown). The nutation signal centered at 20 MHz is in agreement with values predicted for a S = 2 system, as provided by the high-spin Mn(III) species. According to Stoll et al. the nutation frequency ν_{TN} for S > ½ with isotropic g, $B_{ZFS} >> B_1$, $B_{Zeeman} >> B_{ZFS}$ and a transition $|S, m'_S> \leftrightarrow |S, m_S>$ is described by $\nu_{TN} = [S(S+1)-m_S m'_S]^{1/2}\nu_1$, in which ν_1 denotes the nutation frequency of a S = ½ system.[15] Thus, based on ν_1 determined by reference measurements, the transitions between (0, ±1) and (±1, ±2) m_S sublevels are theoretically expected at 22 MHz and 18 MHz in good agreement with the experimental value of approx. 20 MHz. It should be noted that these ideal values only hold for the limiting case that $B_{ZFS} >> B_1$. Figure 5c and Figure 5d show the intensity distribution in the nutation frequency range of the S = ½ and S = 2 species for the reduced and re-oxidized catalyst, respectively. The field range of the signal centered around 20 MHz corresponds well to the broad signal observed in the FSE spectra confirming its assignment to high-spin Mn(III) species (S = 2). It should be emphasized that the

FSE and TN detected Mn(III) species clearly differ from Mn(III) in magnetically ordered phases: At the measurement temperature of 20 K, Mn(III) in ferrimagnetically ordered Mn_3O_4 is expected to yield a typical ferromagnetic signal, while Mn(III) species in the Mn_2O_3 and/or $MnMn_6SiO_{12}$ phase are antiferromagnetically ordered at this temperature and thus, EPR silent. Moreover, the FSE and TN detected Mn(III) species exhibit sufficiently long T_2 relaxation times to enable echo-detection, which requires rather isolated spin centers. Compared to the FSE and TN detected Mn(III) species, a clearly different intensity distribution is observed for the S = ½ species. The width of the distribution (≥ 150 mT) is surprisingly broad and spans a range of g-values from approx. 1.85 to 2.08. Presumably, anisotropic Zeeman and hyperfine interaction (hfi) contribute to the observed line shape and width of the S = ½ species. It should be noted that the cw EPR spectra do not show clear signals due to these species identified by the TN experiments. From Figure 5c and Figure 5d, it becomes apparent that the S = 2 species assigned to high-spin Mn(III) are basically unaffected by the redox reaction. In view of the strong restructuring of the catalyst upon re-oxidation, it is surprising that these presumably rather isolated Mn(III) species remain largely unaffected, while other Mn(III) species associated with long-range magnetically ordered phases in the re-oxdized catalyst undergo massive changes in the redox reaction. A possible explanation for this behavior is a location of these species in a region of the catalyst, which is not altered during the redox cycle. A possible candidate is the silica support. For the latter it was shown that a heating of the initially prepared catalysts containing Na leads to a recrystallization of the silica support into a α-cristobalite phase.[1-2, 11, 46] It is well conceivable that Mn(III) ions are incorporated into the silica phase during the restructuring. In contrast, the signal intensity of the TN and FSE detected S = ½ species increases after re-oxidation of the catalyst demonstrating its accessibility for oxidation by O_2 from the gas phase. However, the shape and width of the S = ½ signal are similar for both the reduced and the re-oxidized catalyst, which indicate that the

corresponding species or the distribution of species giving rise to the spectrum are not significantly altered within the redox cycle. As previously noted the change in signal intensity can be either due to a change in relaxation times and/or in concentration of the species. As similar T_1 and T_2 relaxation times were measured for both the reduced and re-oxidized sample, the lower FSE signal intensity detected for the Mn-Na_2WO_4/SiO_2 catalyst reduced with CH_4 compared to the re-oxdized catalyst can be attributed to a reversible reduction of these S = ½ species by reaction with CH_4. However, it becomes also clear that reaction with CH_4 does not result in a complete depletion of these S = ½ species as demonstrated by the presence of the S = ½ signals also for the reduced catalyst.

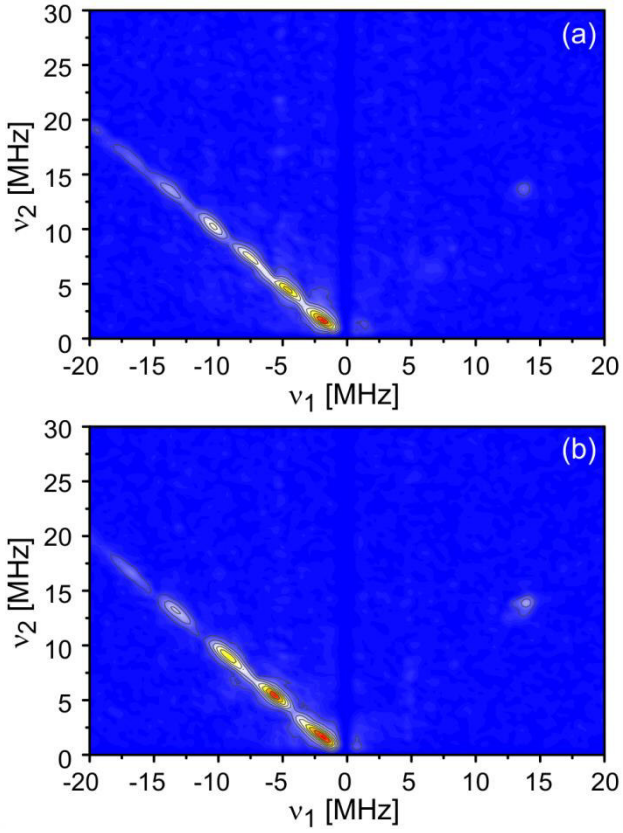

Figure 6. 34 GHz HYSCORE measurements at 20 K with the magnetic field set to 1200 mT of (a) the reduced and (b) the re-oxidized Mn-Na_2WO_4/SiO_2 catalyst.

To obtain further information about the environment of the FSE detected species, 34 GHz 2D HYSCORE measurements aiming at elucidating nuclear spins in the surrounding of the electron spin center were performed with the magnetic field set to maximum peak intensity (1200 mT). The HYSCORE spectra for the reduced and the re-oxidized silica gel supported Mn-Na_2WO_4 catalyst are shown in Figure 6. In the (-,+) quadrant strong signals on the anti-diagonal are observed. While the interpretation of the strong anti-diagonal signals is not evident, the presence of signals in the (-,+) quadrant indicates dominant hfi and/or nuclear quadrupole interaction which may presumably be due to interaction with ^{183}W and/or ^{29}Si based on the observed frequencies. In the (+,+) quadrant, a narrow signal at the free NMR frequency of ^{23}Na is detected whose relative intensity increases for the re-oxidized catalyst suggesting that the S = ½ center is surrounded by Na.

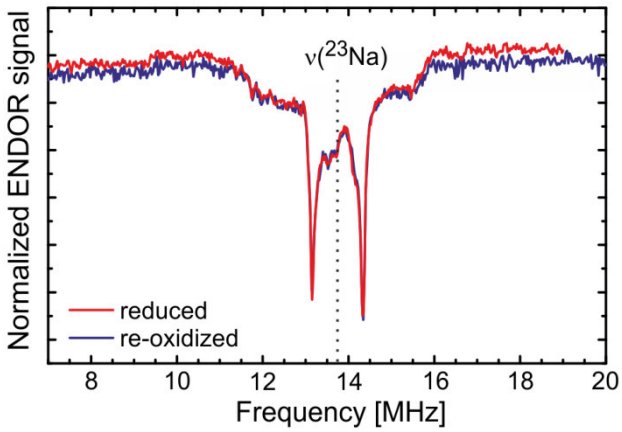

Figure 7. 34 GHz Mims-ENDOR spectra at 20 K with the magnetic field set to 1220 mT of the reduced and the re-oxidized Mn-Na_2WO_4/SiO_2 catalyst.

Further information on the narrow signal at the free NMR frequency of ^{23}Na can be obtained from Mims ENDOR spectra which were aquired at 20 K with the magnetic field set to 1220 mT (see Figure 7). The ENDOR intensities for the reduced and re-oxidized sample are in qualitative agreement with the HYSCORE results. Focussing on the spectral shape, the normalized ENDOR

spectra of the reduced and re-oxidized sample exhibit a very similar line shape. The observed powder pattern is characteristic for dipolar hfi with axial symmetry and negligible isotropic coupling centered at the ^{23}Na nuclear frequency. The observation of such a powder pattern indicates efficient orientational averaging presumably due to a lack of orientational selection at the chosen field position. Furthermore, the spectra lack additional features expected for a high spin state, which provides clear evidence for coupling of Na nuclei to the S = ½ state in line with the observed intensity changes mentioned above.[50] It is, however, important to note, that the chemical environment of the site as probed by ENDOR spectroscopy is not altered by the oxidation/reduction cycle despite the significant changes in the overall composition of the system and the amount of these species.

In the FSE spectra also weak narrow features with regular line spacings were observed in both reduced and re-oxidized samples, which become more apparent in the numerically differentiated FSE spectra shown in Figure 8a. These patterns are also found in the 34 GHz cw EPR spectra, which are clearly seen when the broad main signal is subtracted as shown for the re-oxidized sample in Figure 8b. Spectral simulation suggests that the observed narrow line signals originate from a superposition of different Mn(IV) (S = 3/2, I = 5/2) species exhibiting a typical sextet hfi pattern with isotropic hfi constants A in the range between 195 MHz and 220 MHz and isotropic g-values between 2.010 and 2.073. A quite good agreement with the experimental spectra was obtained assuming the existence of four different Mn(IV) species (see Figure 8b). The corresponding g and A values are summarized in Table 1. In the investigated samples no isolated Mn(II) species were detected. Comparison of the spectra of the reduced and the re-oxidized catalyst clearly demonstrates that the Mn(IV) species are present in both samples at comparable concentrations. Thus, similar to the FSE detected Mn(III) species, these highly oxidized Mn(IV) species remain largely unaffected by the redox reaction despite the restructuring of the catalyst

during re-oxidation. The observation of highly oxidized Mn(IV) species even after reaction in reducing CH_4 atomsphere moreover strongly suggests that these isolated Mn(IV) centers present in small concentration are largely inaccessible from the gas phase, which suggests a location within or close to the SiO_2 support as suggested for the FSE detected Mn(III) species.

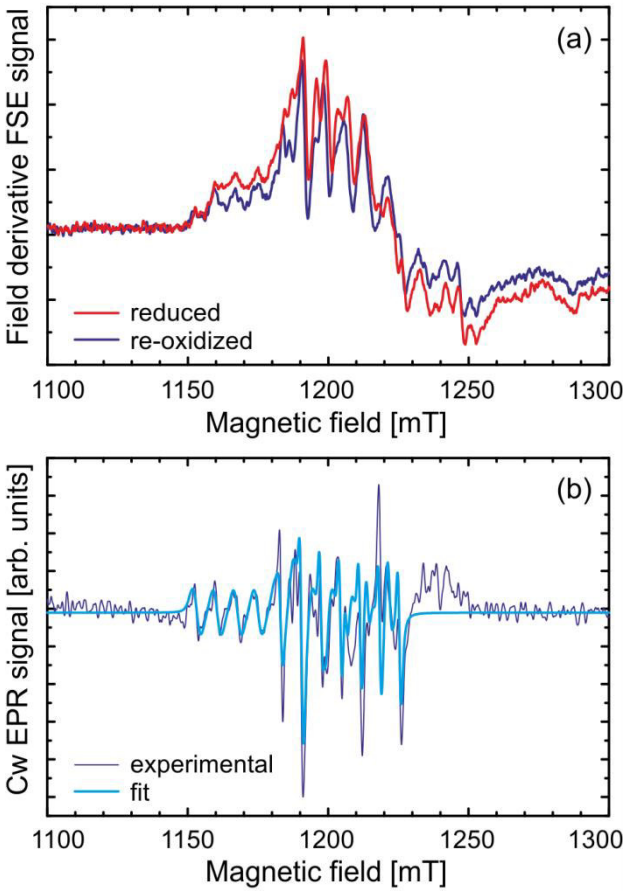

Figure 8. (a) Numerically differentiated experimental 34 GHz FSE spectra (smoothed) obtained at 20 K for the reduced and re-oxidized Mn-Na_2WO_4/SiO_2 catalyst. (b) Comparison of 34 GHz cw EPR experimental spectrum of the re-oxidized sample obtained at room temperature and EasySpin simulation results assuming four different Mn(IV) (S = 3/2, I = 5/2) species. To achieve a nearly flat baseline for the simulation, the main broad signal of the cw EPR spectra was subtracted using a Lorentzian lineshape.

Table 1. Parameters obtained from EasySpin simulation of the 34 GHz cw EPR measurement obtained at room temperature shown in Figure 8b assuming four different Mn(IV) species (S = 3/2, I = 5/2). Given are the g-value, the hfi parameter A and the relative weight.

	g	A [MHz]	weight
A	2.010	197	22 %
B	2.014	195	36 %
C	2.020	219	15 %
D	2.073	211	27 %

An open question is the nature of the FSE detected S = ½ species. Previously, W species were suggested to participate in the redox reaction.[3, 7-8] While transient and short lived paramagnetic W species formed during the reaction at high temperature as suggested by Li[3] are impossible to detect by EPR performed at low temperatures and high spin W(IV) is a S = 1 species, stable W(V) could be a possible candidate for the FSE detected S = ½ center. Yet, (isolated) W(V) are expected at g-values ranging from 1.5 to 1.8 according to results in WO_3.[51-54] In addition, reduction of the W(VI) containing oxidized catalyst should result in an increase of W(V) species, which is opposite to the observed behavior rendering the assignment of the S = ½ center to W(V) unlikely. Another option would be a very highly oxidized Mn(VI) (S = ½) species. This would require this species to survive the reductive treatment of the sample, which is unlikely given the fact that most of the Mn in the reduced catalyst was assigned to Mn(II). Another option for the FSE detected species are exchange coupled clusters with an effective spin of S = ½ whose concentration is altered depending on the gas phase composition and wich are surrounded by a Na-containing diamagnetic material. As Mn(II), Mn(III) and Mn(IV) are stable species in both the reduced and re-oxidized catalyst, both double exchanged coupled Mn(II)-O-Mn(III) and/or

Mn(III)-O-Mn(IV)[55-56] sites in their lowest spin state are possible candidates for the S = ½ centers with a surprisingly large linewidth (150 mT). A possible location of such an isolated cluster would be at the interface of a Na_2WO_4 phase and the Na containing SiO_2[11, 46] support.

4. CONCLUSION

Reduction with CH_4 and reoxidation with O_2 of Mn-Na_2WO_4/SiO_2 under reaction conditions leads to significant changes in the magnetic properties of the catalyst detected by EPR and SQUID magnetization measurements, using samples sealed off under inert conditions. These experiments demonstrated the presence of a variety of Mn species in different oxidation states as well as their role in the oxygen storage capability of the catalyst. However, no evidence for the presence of reduced W species neither W(V) nor (high-spin) W(IV) centers could be found in this investigation.

Long-range ordered magnetic phases consistent with nano-sized Mn_3O_4 as well as Mn_2O_3 and/or $MnMn_6SiO_{12}$ were detected upon re-oxidation implying a strong involvement of these Mn species in the oxygen storage. Changes in susceptibility as well as EPR properties confirm a massive restructuring compared to the state of the reduced catalyst consistent with the existence of disordered or defect-rich Mn(II) containing clusters.

Isolated Mn(III) and Mn(IV) species were also identified, which are clearly not involved in the oxygen storage of the catalyst, suggesting their location rather buried presumably in the SiO_2 support and thus, inaccessible to chemistry invoked by CH_4 or O_2 impinging from the gas phase.

Next to species clearly attributed to Mn because of hyperfine or finestructure properties, a paramagnetic center with effective S = ½ spin was found whose concentration depended on the oxidation state of the catalyst. In light of their chemical properties, these signals were tentatively

assigned to exchange coupled clusters e.g. Mn(II)-O-Mn(III) and/or Mn(III)-O-Mn(IV) pairs in their low spin configuration.

AUTHOR INFORMATION

Corresponding Author

*E-mail: wiebke.riedel@fu-berlin.de. Phone: +49 30 83855307

Notes

The authors declare no competing financial interest.

SUPPORTIG INFORMATION

Temperature dependence of cw EPR line width for the reduced Mn-Na_2WO_4/SiO_2 catalyst and of the (double) integrated intensity of the cw EPR signals for the reduced and re-oxidized Mn-Na_2WO_4/SiO_2 catalyst as well as the change in cw EPR line shape observed for the re-oxidized sample for measurements at 100 K and 80 K.

This material is available free of charge via the Internet at http://pubs.acs.org.

ACKNOWLEDGEMENTS

The authors gratefully acknowledge financial support by the DFG through the center of excellence “Unicat” hosted at the TU Berlin and DFG SPP 1601. We like to thank the Quantum Material Corelab at HZB for the magnetization measurements.

REFERENCES

1. Fang, X.; Li, S.; Lin, J.; Chu, Y. Oxidative Coupling of Methane on W-Mn Catalysts, *J. Mol. Catal. (in Chinese)* **1992**, *6*, 427-433.

2. Fang, X.; Li, S.; Lin, J.; Gu, J.; Yan, J. D. Preparation and Characterization of W-Mn Catalyst for Oxidative Coupling of Methane, *J. Mol. Catal. (in Chinese)* **1992**, *8*, 255-262.

3. Li, S. B. Oxidative Coupling of Methane over W-Mn/SiO_2 Catalyst. *Chin. J. Chem.* **2001**, *19*, 16-21.

4. Sadjadi, S.; Jaso, S.; Godini, H. R.; Arndt, S.; Wollgarten, M.; Blume, R.; Görke, O.; Schomäcker, R.; Wozny, G.; Simon, U. Feasibility Study of the Mn-Na_2WO_4/SiO_2 Catalytic System for the Oxidative Coupling of Methane in a Fluidized-Bed Reactor. *Catal. Sci. Technol.* **2015**, *5*, 942-952.

5. Fleischer, V.; Littlewood, P.; Parishan, S.; Schomäcker, R. Chemical Looping as Reactor Concept for the Oxidative Coupling of Methane over a Na_2WO_4/Mn/SiO_2 Catalyst. *Chem. Engin. J.* **2016**, *306*, 646-654.

6. Fleischer, V.; Simon, U.; Parishan, S.; Colmenares, M. G.; Görke, O.; Gurlo, A.; Riedel, W.; Thum, L.; Risse, T., Dinse, K.-P., et al. Investigation of the Role of the Na_2WO_4/Mn/SiO_2 Catalyst Composition in the Oxidative Coupling of Methane by Chemical Looping Experiments. *J. Catal.* **2018**, *360*, 102-117.

7. Wu, J. G.; Li, S. B.; Niu, J. Z.; Fang, X. P. Mechanistic Study of Oxidative Coupling of Methane over Mn_2O_3-Na_2WO_4/SiO_2 Catalyst. *Appl. Catal. A* **1995**, *124*, 9-18.

8. Jiang, Z. C.; Gong, H.; Li, S. B. Methane Activation over Mn_2O_3-Na_2WO_4/SiO_2 Catalyst and Oxygen Spillover. *Stud. Surf. Sci. Catal.* **1997**, *112*, 481-490.

9. Ji, S. F.; Xiao, T. C.; Li, S. B.; Xu, C. Z.; Hou, R. L.; Coleman, K. S.; Green, M. L. H. The Relationship between the Structure and the Performance of Na-W-Mn/SiO_2 Catalysts for the Oxidative Coupling of Methane. *Appl. Catal. A* **2002**, *225*, 271-284.

10. Koirala, R.; Büchel, R.; Pratsinis, S. E.; Baiker, A. Oxidative Coupling of Methane on Flame-Made Mn-Na_2WO_4/SiO_2: Influence of Catalyst Composition and Reaction Conditions. *Appl. Catal. A* **2014**, *484*, 97-107.

11. Simon, U.; Görke, O.; Berthold, A.; Arndt, S.; Schomäcker, R.; Schubert, H. Fluidized Bed Processing of Sodium Tungsten Manganese Catalysts for the Oxidative Coupling of Methane. *Chem. Engin. J.* **2011**, *168*, 1352-1359.

12. Wang, J. X.; Chou, L. J.; Zhang, B.; Song, H. L.; Zhao, J.; Yang, J.; Li, S. B. Comparative Study on Oxidation of Methane to Ethane and Ethylene over Na_2WO_4-Mn/SiO_2 Catalysts Prepared by Different Methods. *J. Mol. Catal. A Chem.* **2006**, *245*, 272-277.

13. Fleischer, V.; Steuer, R.; Parishan, S.; Schomäcker, R. Investigation of the Surface Reaction Network of the Oxidative Coupling of Methane over Na_2WO_4/Mn/SiO_2 Catalyst by Temperature Programmed and Dynamic Experiments. *J. Catal.* **2016**, *341*, 91-103.

14. Liu, Y.; Hou, R. L.; Liu, X. X.; Xue, J. Z.; Li, S. B. Performance of Na_2WO_4-Mn/SiO_2 Catalyst for Conversion of CH_4 with CO_2 into C_2 Hydrocarbons and Its Mechanism. *Stud. Surf. Sci. Catal.* **1998**, *119*, 307-311.

15. Stoll, S.; Jeschke, G.; Willer, M.; Schweiger, A. Nutation-Frequency Correlated EPR Spectroscopy: The PEANUT Experiment. *J. Magnet. Res.* **1998**, *130*, 86-96.

16. Dinse, A.; Wolfram, T.; Carrero, C.; Schlögl, R.; Schomäcker, R.; Dinse, K.-P. Exploring the Structure of Paramagnetic Centers in SBA-15 Supported Vanadia Catalysts with Pulsed One- and Two-Dimensional Electron Paramagnetic Resonance (EPR) and Electron Nuclear Double Resonance (ENDOR). *J. Phys. Chem. C* **2013**, *117*, 16921-16932.

17. Lopez-Ortega, A.; Tobia, D.; Winkler, E.; Golosovsky, I. V.; Salazar-Alvares, G.; Estrade, S.; Estrader, M.; Sort, J.; Gonzales, M.A.; Surinach, S., et al. Size-Dependent Passivation Shell and Magnetic Properties in Antiferromagnetic/Ferrimagnetic Core/Shell MnO Nanoparticles. *J. Am. Chem. Soc.* **2010**, *132*, 9398-9407.

18. Golosovsky, I. V.; Arcon, D.; Jaglicic, Z.; Cevc, P.; Sakhnenko, V. P.; Kurdyukov, D. A.; Kumzerov, Y. A. ESR Studies of MnO Embedded into Silica Nanoporous Matrices with Different Topology. *Phys. Rev. B* **2005**, *72,* 144410.

19. Sako, S.; Ohshima, K. Antiferromagnetic Transition Temperatur of MnO Ultrafine Particle. *J. Phys. Soc. Jpn.* **1995**, *64*, 944-950.

20. Muthamizh, S.; Suresh, R.; Giribabu, K.; Manigandan, R.; Kumar, S. P.; Munusamy, S.; Narayanan, V. $MnWO_4$ Nanocapsules: Synthesis, Characterization and Its Electrochemical Sensing Property. *J. Alloy. Comp.* **2015**, *619*, 601-609.

21. Jacobs, I. S. Evidence for Triangular Moment Arragements in $MnO.Mn_2O_3$. *J. Phys.Chem. Solids* **1959**, *11*, 1-11.

22. Dwight, K.; Menyuk, N. Magnetic Properties of Mn_3O_4 and the Canted Spin Problem. *Phys. Rev.* **1960**, *119*, 1470-1479.

23. Tseng, L. T.; Lu, Y. H.; Fan, H. M.; Wang, Y. R.; Luo, X.; Liu, T.; Munroe, P.; Li, S.; Yi, J. B. Magnetic Properties in α-MnO_2 Doped with Alkaline Elements. *Sci. Rep.* **2015**, *5*, 9094.

24. Stobbe, E. R.; de Boer, B. A.; Geus, J. W. The Reduction and Oxidation Behaviour of Manganese Oxides. *Catal. Today* **1999**, *47*, 161-167.

25. Buciuman, F.; Patcas, F.; Craciun, R.; Zahn, D. R. T. Vibrational Spectroscopy of Bulk and Supported Manganese Oxides. *Phys. Chem. Chem. Phys.* **1999**, *1*, 185-190.

26. Chevalier, R. R.; Roult, G.; Bertaut, E. F. Etude Par Effet Mössbauer Du Systeme $Mn_{2-X}Fe_xO_3$ Et Transitions Magnetiques Dans Mn_2O_3 Par Diffraction Neutronique. *Solid State Commun.* **1967**, *5*, 7-11.

27. Geller, S.; Grant, R. W.; Cape, J. A.; Espinosa, G. P. Magnetic Behavior of the System Mn_2O_3-Fe_2O_3. *J. Appl. Phys.* **1967**, *38*, 1457-1458.

28. Grant, R. W.; Geller, S.; Cape, J. A.; Espinosa, G. P. Magnetic and Crystallographic Transitions in the α-Mn_2O_3-Fe_2O_3 System. *Phys. Rev.* **1968**, *175*, 686-695.

29. Ohmann, S.; Abs-Wurmbach, I.; Stusser, N.; Sabine, T. M.; Westerholt, K. The Magnetic Structure of Braunite $Mn^{2+}Mn^{3+6}O_8/SiO_4$. *Z. Kristall.* **1998**, *213*, 19-27.

30. Abs-Wurmbach, I.; Ohmann, S.; Westerholt, K.; Meier, T.; Mouron, P.; Choisnet, J. Magnetic Phase Diagrams of Mg-, Fe-, (Cu+Ti) and Cu-Substituted Braunite $Mn^{2+}Mn^{3+6}SiO_{12}$. *Phys. Chem. Miner.* **2002**, *29*, 280-290.

31. Ohama, N.; Hamaguchi, Y. Determination of the Exchange Integrals in β-MnO_2. *J. Phys. Soc. Jpn.* **1971**, *30*, 1311-1318.

32. Wang, G. L.; Tang, B.; Zhuo, L. H.; Ge, J. C.; Xue, M. Facile and Selected-Control Synthesis of β-MnO_2 Nanorods and Their Magnetic Properties. *Europ. J. Inorg. Chem.* **2006**, 2313-2317.

33. Luo, J.; Zhu, H. T.; Liang, J. K.; Rao, G. H.; Li, J. B.; Du, Z. M. Tuning Magnetic Properties of α-MnO_2 Nanotubes by K^+ Doping. *J. Phys. Chem. C* **2010**, *114*, 8782-8786.

34. Lee, Y. C.; Pakhomov, A. B.; Krishnan, K. M. Size-Driven Magnetic Transitions in Monodisperse MnO Nanocrystals. *J. Appl. Phys.* **2010**, *107*, 09E124.

35. Parmigiani, F.; Sangaletti, L. Fine Structures in the X-Ray Photoemission Spectra of MnO, FeO, CoO, and NiO Single Crystals. *J. Electr. Spectr. Rel. Phen.* **1999**, *98*, 287-302.

36. Lines, M. E.; Jones, E. D. Antiferromagnetism in the Face-Centered Cubic. II. Magnetic Properties of MnO. *Phys. Rev.* **1965**, *139*, A1313.

37. Taniguchi, K.; Abe, N.; Takenobu, T.; Iwasa, Y.; Arima, T. Ferroelectric Polarization Flop in a Frustrated Magnet $MnWO_4$ Induced by a Magnetic Field. *Phys. Rev. Lett.* **2006**, *97*.

38. Arkenbout, A. H.; Palstra, T. T. M.; Siegrist, T.; Kimura, T. Ferroelectricity in the Cycloidal Spiral Magnetic Phase of $MnWO_4$. *Phys. Rev. B* **2006**, *74*, 184431.

39. Heyer, O.; Hollmann, N.; Klassen, I.; Jodlauk, S.; Bohaty, L.; Becker, P.; Mydosh, J. A.; Lorenz, T.; Khomskii, D. A New Multiferroic Material: $MnWO_4$. *J. Phys. Condens. Matter* **2006**, *18*, L471-L475.

40. Kundys, B.; Simon, C.; Martin, C. Effect of Magnetic Field and Temperature on the Ferroelectric Loop in $MnWO_4$. *Phys. Rev. B* **2008**, *77*, 172402.

41. Felea, V.; Lemmens, P.; Yasin, S.; Zherlitsyn, S.; Choi, K. Y.; Lin, C. T.; Payen, C. Magnetic Phase Diagram of Multiferroic $MnWO_4$ Probed by Ultrasound. *J. Phys. Cond. Matt.* **2011**, *23*, 216001.

42. Chen, Z. W.; Zhang, S. Y.; Tan, S.; Li, F. Q.; Wang, J.; Jin, S. Z.; Zhang, Y. H. Preparation and Electron Spin Resonance Effect of Nanometer-Sized Mn_2O_3. *J. Cryst. Growth* **1997**, *180*, 280-283.

43. Mukherjee, S.; Pal, A. K.; Bhattacharya, S.; Raittila, J. Magnetism of Mn_2O_3 Nanocrystals Dispersed in a Silica Matrix: Size Effects and Phase Transformations. *Phys. Rev. B* **2006**, *74*, 104413.

44. Javed, Q. U.; Wang, F. P.; Rafique, M. Y.; Toufiq, A. M.; Iqbal, Z. Canted Antiferromagnetic and Optical Properties of Nanostructures of Mn_2O_3 Prepared by Hydrothermal Synthesis. *Chin. Phys. B* **2012**, *21*, 117311.

45. Mukherjee, S.; Yang, H. D.; Pal, A. K.; Majumdar, S. Magnetic Properties of MnO Nanocrystals Dispersed in a Silica Matrix. *J. Magnet. Magnet. Mater.* **2012**, *324*, 1690-1697.

46. Palermo, A.; Vazquez, J. P. H.; Lee, A. F.; Tikhov, M. S.; Lambert, R. M. Critical Influence of the Amorphous Silica-to-Cristobalite Phase Transition on the Performance of $Mn/Na_2WO_4/SiO_2$ Catalysts for the Oxidative Coupling of Methane. *J. Catal.* **1998**, *177*, 259-266.

47. Stoll, S.; Schweiger, A. Easyspin, a Comprehensive Software Package for Spectral Simulation and Analysis in EPR. *J. Magnet. Res.* **2006**, *178*, 42-55.

48. Schwach, P.; Eichelbaum, M.; Schlögl, R.; Risse, T.; Dinse, K.-P. Evidence for Exchange Coupled Electrons and Holes in MgO after Oxidative Activation of CH_4: A Multifrequency Transient Nutation EPR Study. *J. Phys. Chem. C* **2016**, *120*, 3781-3790.

49. Simon, U.; Alarcón Villaseca, S.; Shang, H.; Levchenko, S. V.; Arndt, S.; Epping, J. D.; Görke, O.; Scheffler, M.; Schomäcker, R.; van Tol, J., et al. Li/MgO Catalysts Doped with Alio-Valent Ions. Part II: Local Topology Unraveled by EPR/NMR and DFT Modeling. *ChemCatChem.* **2017**, *9*, 3597–3610.

50. Weiden, N.; Goedde, B.; Käß, H.; Dinse, K. P.; Rohrer, M. Squeezing of Nitrogen Atomic Orbitals in a Chemical Trap. *Phys. Rev. Lett.* **2000**, *85*, 1544-1547.

51. Gazzinelli, R.; Schirmer, O. F. Light-Induced W^{5+} ESR in WO_3. *J. Phys. C* **1977**, *10*, L145-L149.

52. Pifer, J. H.; Sichel, E. K. Electron Resonance Study of Hydrogen-Containing WO_3 Films. *J. Electron. Mater.* **1980**, *9*, 129-140.

53. Gerard, P.; Deneuville, A.; Courths, R. Characterization of WO_3 Thin Films Before and After Coloration. *Thin Solid Films* **1980**, *71*, 221-236.

54. Schirmer, O. F.; Salje, E. W^{5+} Polaron in Crystalline Low-Temperature WO_3 ESR and Optical Absorption. *Solid State Commun.* **1980**, *33*, 333-336.

55. Magnuson, A.; Liebisch, P.; Högblom, J.; Anderlund, M. F.; Lomoth, R.; Meyer-Klaucke, W.; Haumann, M.; Dau, H. Bridging-Type Changes Facilitate Successive Oxidation Steps at About 1 V in Two Binuclear Manganese Complexes - Implications for Photosynthetic Water-Oxidation. *J. Inorg. Biochem.* **2006**, *100*, 1234-1243.

56. Peng, X.; Guo, Y. Q.; Yin, Q.; Wu, J. C.; Zhao, J. Y.; Wang, C. M.; Tao, S.; Chu, W. S.; Wu, C. Z.; Xie, Y. Double-Exchange Effect in Two-Dimensional MnO_2 Nanomaterials. *J. Amer. Chem. Soc.* **2017**, *139*, 5242-5248.

TOC GRAPHIC

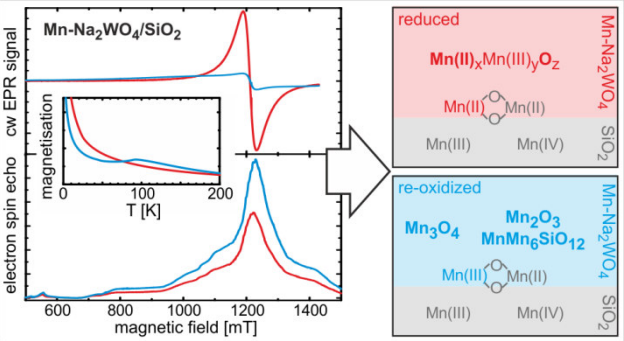
Mn-Na2WO4/SiO2
cw EPR signal
electron spin echo
magnetisation
0
100
200
T [K]
600
800
1000
1200
1400
magnetic field [mT]
reduced
Mn(II)xMn(III)yOz
Mn(II)
Mn(II)
Mn(III)
Mn(IV)
Mn-Na2WO4
SiO2
re-oxidized
Mn3O4
Mn2O3
MnMn6SiO12
Mn(III)
Mn(II)
Mn(III)
Mn(IV)
Mn-Na2WO4
SiO2